J. Fluid Mech. (1976), *vol.* 76, *part* 2, *pp.* 337–362
Printed in Great Britain

Thermoconvective instabilities in a porous medium bounded by two concentric horizontal cylinders

By JEAN-PAUL CALTAGIRONE

Laboratoire d'Aérothermique du C.N.R.S., 4 ter,
Route des Gardes, 92190 Meudon, France

(Received 7 October 1975)

The study of natural convection in a saturated porous medium bounded by two concentric, horizontal, isothermal cylinders reveals different types of evolution according to the experimental conditions and the geometrical configuration of the model. At small Rayleigh numbers the state of the system corresponds to a regime of *pseudo-conduction*. The isotherms are coaxial with the cylinders. At larger Rayleigh numbers a regime of steady two-dimensional convection sets in between the two cylinders. Finally, for Rayleigh numbers above the critical Rayleigh number Ra_c^* the phenomena become three-dimensional and fluctuating. The appearance of these different regimes depends, moreover, on the geometry considered and, in particular, on two numbers: R, the ratio of the radii of the cylinders, and A, the ratio of the length of the cylinders to the radius of the inner one. In order to approach these experimental observations and to obtain realistic theoretical models, several methods of solving the equations have been used.

The perturbation method yields information about the thermal field and the heat transfer between the cylinders under conditions close to the equilibrium state.

A numerical two-dimensional model enables us to extend the range of investigation and to represent properly the phenomena when steady convection appreciably modifies the temperature distribution and the velocities within the porous layer.

Neither of these models allows account to be taken of the instabilities observed experimentally above a critical Rayleigh number Ra_c^*. For this reason, a study of stability has been carried out using a Galerkin method based on equations corresponding to an initial state of steady convection. The results obtained show the importance of three-dimensional effects for the onset of fluctuating convection. The critical transition Rayleigh number Ra_c^* is thus determined in terms of the ratio of the radii R by solving an eigenvalue problem.

A numerical three-dimensional model based on the method of finite elements has thus been developed in order to point out the different types of evolution with time. Steady two-dimensional convection and fluctuating three-dimensional convection have been actually found by calculation. The solution of the system of equations by the method of finite elements is briefly described.

The experimental and theoretical results are then compared and a general physical interpretation is given.

1. Introduction

Numerous experimenters and theoreticians have studied the problem of plane porous layers and pointed out two regimes of convection, one being steady, the other fluctuating (Combarnous & Bories 1975). Furthermore, a significant number of numerical and theoretical models have been developed on this topic. On the other hand, there are very few studies available on natural convection in a porous medium bounded by two cylinders. A numerical study by the author (1972) is also restricted to a diagram, $Nu^* = f(Ra^*, R)$, but the similarity between the phenomena observed in a porous layer and in a fluid layer leads us to expect qualitative similarities to several publications.

Mack & Bishop (1968) have solved the equations defining the steady two-dimensional regime in an annular fluid layer by the perturbation method. These authors expanded the temperature and stream function in power series in Ra^*, considering terms up to the third. Their results are significant for not very large Rayleigh numbers and allow secondary flows to appear in the upper and lower part of the annular layer at very small Prandtl numbers. Perturbation analysis has also been used by Rotem (1971) in the case of surfaces which are not perfectly conducting.

Early numerical calculations concerning the geometry studied have been carried out by Crawford & Lemlich (1962), who used the method of finite differences to solve the equations of continuity, energy and momentum. The range of investigation is restricted to three different values of the ratio of the radii at the Prandtl number 0·714. The numerical study by Abbott (1964) is restricted to small radius ratios and yields nothing new compared with the previous study. The numerical two-dimensional model of Powe, Carley & Carruth (1971) shows the existence of secondary effects, such as vortices rotating in the direction opposite to the main stream. The study of stability developed below will show conclusively that it is impossible to obtain these effects with a two-dimensional model. Several experimental studies have been carried out in order to get quantitative information about the total heat transfer. The results give in general a correlation between the Nusselt number Nu, the Rayleigh number Ra, the Prandtl number Pr and the ratio of the radii R (Liu, Mueller & Landis 1961; Lis 1966). The photographs by Bishop & Carley (1966) show the existence of an oscillatory regime. The period and amplitude of these oscillations are given as a function of the temperature gradient imposed between the cylinders.

However, the most significant results on convection in an annular fluid layer have been obtained by Grigull & Hauf (1966). Using a Mach–Zehnder interferometer for their visualizations, the authors point out different regimes of convection, in particular three-dimensional effects, which are very marked in the upper part of the experimental cell as the Grashof number increases. Furthermore, the local Nusselt number at the surface of the cylinders is calculated from interferograms and a relation $Nu^* = f(Gr, \delta/d_i)$ is given (δ is the difference in the radii and d_i the inner diameter).

Detailed qualitative information is given by Bishop, Carley & Powe (1968) for a regime of oscillating three-dimensional convection, based on observations

made on an annular space filled with air. Visualization was achieved with the help of tobacco smoke. The amplitude and wavelength of these oscillations are given as a function of the Grashof number. For relatively small ratios of the radii ($R = 1{\cdot}15$), Liu *et al.* (1961) find a regime of multicellular convection, the origin of which they impute to the fact that the critical Rayleigh number (1707) has been exceeded in the locally horizontal layer which forms in the upper zone of the annular space. This point of view will be confirmed later on.

To sum up, the experimental studies performed by the different authors clearly demonstrate the appearance of secondary effects superimposed on the steady two-dimensional flow at relatively high values of the Grashof number. But these results are still fragmentary and do not enable us to define the criteria for the onset of these effects and the shape of the thermoconvective cells. Moreover, the theoretical models and numerical calculations are not quite consistent.

However, these different investigations carried out in a fluid layer enable us to make qualitative comparisons and will confirm, once more, the similarity of these phenomena to those in porous media.

Chronologically, the study of natural convection in a porous medium bounded by two indefinite concentric cylinders has been developed as follows. Visualization experiments using the Christiansen effect carried out in a cell of small thickness (2 cm) have revealed three-dimensional effects superimposed on the main two-dimensional motion in the upper part of the annular space. The use of an experimental cell of great longitudinal extent (length of the cylinders = 80 cm, outside diameter = 16 cm) made it possible to obtain these secondary effects: as the temperature field became three-dimensional, fluctuations were found to occur in the upper part of the cell, whereas the lower zone remained two-dimensional. In order to demonstrate these instabilities a numerical model has been constructed. It is composed of a two-dimensional network and the equations for the energy and the momentum transformed into difference form. Even at very large Rayleigh numbers no instabilities are to be found by calculation: the temperature field and streamlines are steady and symmetric about a vertical axis passing through the centre of the cylinders. A study of stability using the Galerkin method shows that the secondary fluctuating effect can not be obtained if the third dimension is not considered. The critical Rayleigh number Ra_c^* for the occurrence of fluctuating convection is found as a function of the radius ratio and the aspect ratio in the direction perpendicular to the cylinder cross-section.

Some calculations carried out using a numerical three-dimensional model based on the finite-element method have confirmed the existence of spiral unsteady thermoconvective flows. This chronological order has been followed in this paper and a physical interpretation of the results is given.

2. Formulation of the problem

Let us consider an annular porous layer of length L bounded by an inner cylinder of radius r_i and an outer cylinder of radius r_o. Two characteristic parameters are defined: $R = r_o/r_i$, the ratio of the radii, and $A = L/r_i$, the

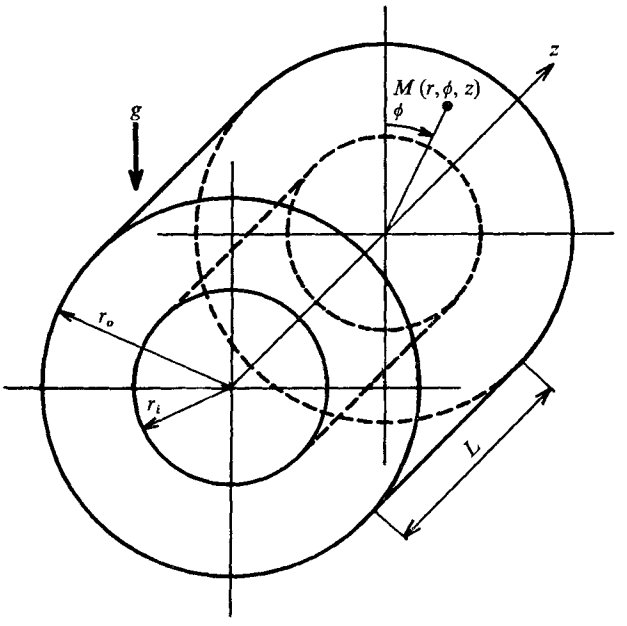

FIGURE 1. Representation of the model with geometrical characteristics.

longitudinal aspect ratio of the layer. Figure 1 shows the different geometrical quantities and notation used below.

The porous matrix is characterized by its porosity ϵ and its permeability K; α is the thermal expansion coefficient of the saturating fluid, $(\rho c)_f$ its heat capacity, and ν its coefficient of kinematic viscosity. The porous medium formed by the porous matrix and the interstitial fluid is treated as a fictitious isotropic fluid with heat capacity $(\rho c)^* = \epsilon(\rho c)_f + (1-\epsilon)(\rho c)_s$ (where $(\rho c)_s$ is the heat capacity of the solid) and thermal conductivity λ^*. The physical properties of the medium are regarded as constant, in particular with respect to temperature dependence. The variations in density with temperature are neglected, except with regard to their influence on the buoyancy force (Boussinesq's approximation).

The inner and outer cylinders are assumed to be isothermal and are held at the temperatures T_i and T_o, respectively, with $T_i > T_o$. The physical constants are evaluated at the average temperature $T_m = \frac{1}{2}(T_i + T_o)$. The equations for mass conservation, energy and momentum governing phenomena in a porous medium may be written as follows for an incompressible fluid:

$$\nabla . \mathbf{V} = 0, \tag{1}$$

$$(\rho c)^* \partial_t T - \lambda^* \nabla^2 T + (\rho c)_f \mathbf{V} . \nabla T = 0, \tag{2}$$

$$\epsilon^{-1} \rho \, \partial_t \mathbf{V} + \nabla p - \rho \mathbf{g} + \rho \nu K^{-1} \mathbf{V} = 0, \tag{3}$$

where $\mathbf{g} = -g \cos\phi \mathbf{e}_1 + g \sin\phi \mathbf{e}_2$ is the gravitational acceleration,

$$\mathbf{V} = V_r \mathbf{e}_1 + V_\phi \mathbf{e}_2 + V_z \mathbf{e}_3$$

is the filtration velocity, $\rho = \rho_0[1 - \alpha(T - T_0)]$ is the equation of state and p is the pressure; $\mathbf{e}_1$, $\mathbf{e}_2$ and $\mathbf{e}_3$ are unit vectors.

The cylindrical co-ordinates are referred to the radius r_i, the time to the quantity $(\rho c)^* r_i^2/\lambda^*$, the temperature to ΔT, the velocity to $\lambda^*/r_i(\rho c)_f$ and the pressure to $\lambda^*\mu/K(\rho c)_f$. This yields for the reduced quantities

$$\partial_t T - \nabla^2 T + \mathbf{V}.\nabla T = 0, \tag{4}$$

$$\epsilon^{-1} Pr^{*-1} M^{-1} F \partial_t \mathbf{V} + \nabla p + Ra^* \mathbf{k} T - Ra^* Ga \mathbf{k} + \mathbf{V} = 0, \tag{5}$$

with $\mathbf{k} = -\cos\phi \mathbf{e}_1 + \sin\phi \mathbf{e}_2$. Five dimensionless numbers appear in (4) and (5) together with the porosity ϵ. These are the Rayleigh number Ra^*, the Prandtl number Pr^* and three characteristic numbers of the porous medium and of the experimental conditions, F, M and Ga, respectively:

$$Ra^* = g\alpha(\rho c)_f \Delta T K r_i/\lambda^* \nu, \quad Pr^* = \nu(\rho c)_f/\lambda^*,$$
$$F = K/r_i^2, \quad M = (\rho c)_f/(\rho c)^*, \quad Ga = 1/\alpha \Delta T.$$

The number F, which represents the fineness of the porous medium compared with a characteristic dimension, takes very small values when the porous medium is of small granulometry (of about 10^{-6} to 10^{-8}). On the other hand, previous numerical calculations (Caltagirone 1975*a*) have shown the negligible influence of this number when lower than 10^{-3}. With the approximation $F = 0$ the momentum equation (5) reduces to Darcy's law. Finally, we have

$$\partial_t T - \nabla^2 T + \mathbf{V}.\nabla T = 0, \tag{6}$$

$$\nabla p + Ra^* \mathbf{k} T - Ra^* Ga \mathbf{k} + \mathbf{V} = 0. \tag{7}$$

From the energy equation (6) and Darcy's equation (7) a numerical model of the problem can be developed successively for a two- and three-dimensional space.

3. Experiments

The early experimental results on the problem of the annular layer bounded by two concentric horizontal cylinders were obtained by a method of visualization of the thermal field using the Christiansen effect (Cloupeau & Klarsfeld 1973; Caltagirone 1971). The optical method used is based on the fact that the porous medium formed by a granulous, transparent, homogeneous, isotropic solid, such as glass powder, and a colourless liquid with a refraction coefficient near that of the solid is optically homogeneous only for the wavelength λ_c. Owing to the differences between the dispersion curves $n_f = f(\lambda_c)$ and $n_s = g(\lambda_c)$ of the liquid and solid, respectively, the central wavelength λ_c is a function of the temperature. The mixture having been previously calibrated ($\lambda_c = h(T)$), the experimental cell is illuminated by an arc lamp producing a set of spectrum lines. The lines with different colours represent the isotherms.

The longitudinal aspect ratio of the cell A is 0·5, and the ratio of the radii R is 2. When the Rayleigh number exceeds a certain value estimated to be about 70, the thermal field, which was previously two-dimensional, becomes three-dimensional. The secondary effects are located in the upper part of the cell. As the cell for visualization does not yield precise information on the heat transfer between the cylinders, an experimental cell has been constructed ($L = 80$ cm, $r_i = 4$ cm, $r_o = 8$ cm; i.e. $A = 20$ and $R = 2$). The experimental cell is formed of

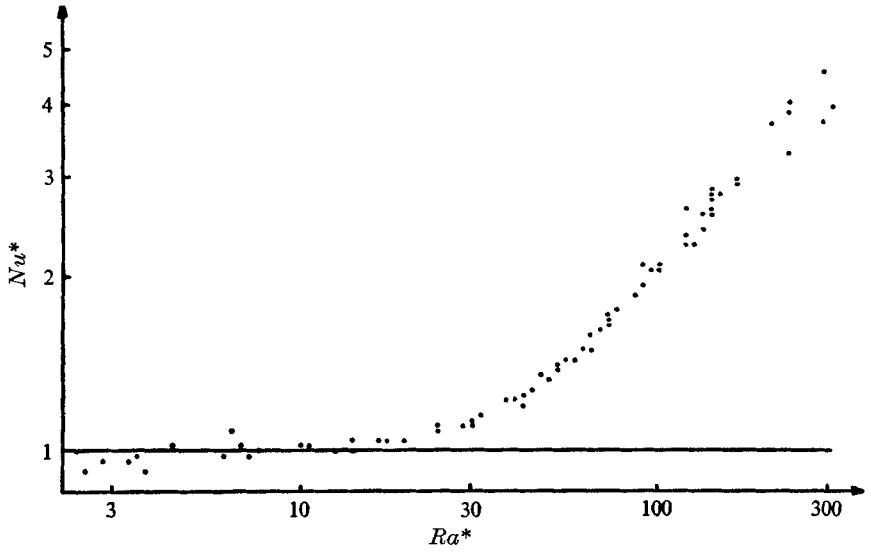

FIGURE 2. Experimental results obtained at $R = 2$.

an inner cylinder heated by six resistances fed by a stabilized d.c. generator (40V, 100A) and of an outer cylinder cooled by water flowing at high speed in an outer jacket. Two Makrolon supports 8 cm thick reduce the heat losses at the ends of the cell.

The temperature measurements are achieved by means of 16 thermocouples placed in alumina cans 2 mm in diameter and 1 m in length allowing them to be introduced and positioned in the porous layer.

The value of the apparent thermal conductivity of the porous medium is measured for a small temperature difference maintained between the cylinders. In this case, the Rayleigh number is small ($Ra^* < 8$ at $R = 2$) and heat exchanges occur by conduction; this is why λ^* is calculated for a permanent regime. The other physical constants are taken from the literature.

A data acquisition system collects the different parameters, such as the supply voltage, the current, the electromotive forces of the thermocouples, etc. and transcribes them either on a printer or to a band perforator. The data are processed on a computer and for each experiment the Rayleigh and Nusselt numbers are calculated and the heat losses estimated. The different correlations are also printed. The experimental results given here are by no means exhaustive, because the experiments carried out are still only partial and limited to one ratio of the radii ($R = 2$) and to one type of porous medium (glass balls and water).

Three regimes of convection are observed, each of them corresponding to a part of the curve $Nu^* = f(Ra^*)$ of figure 2.

(i) A range where the Rayleigh number is lower than 8 and where the convective phenomena are very little developed, the heat transfer occurring only by conduction ($Nu^* = 1$). The temperature field is two-dimensional and steady. This regime will be called *pseudo-conduction*.

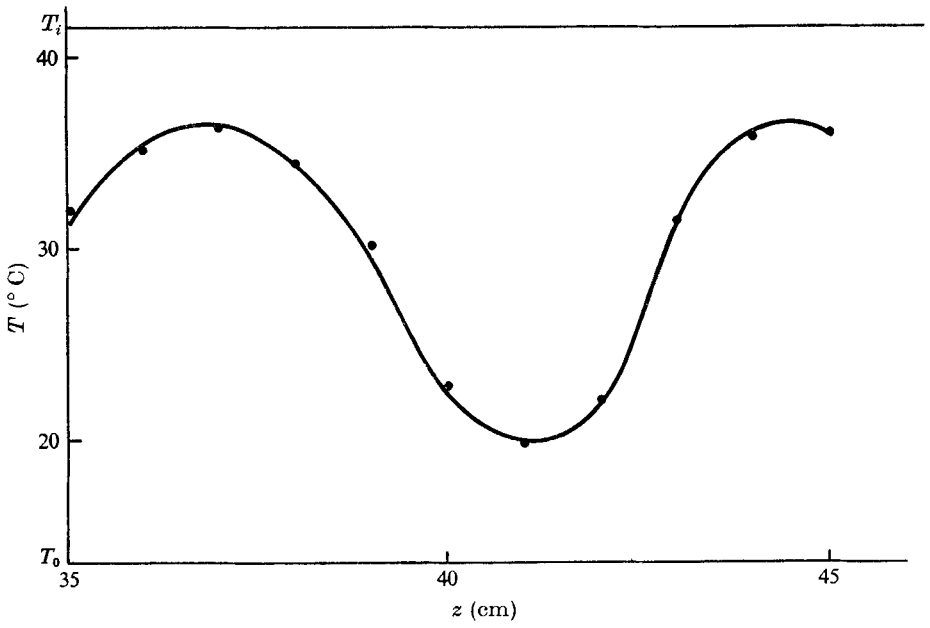

FIGURE 3. Temperature variation along a generatrix ($r = 1{\cdot}5$; $\phi = 0$) with $Ra^* = 157$, $R = 2$.

(ii) In the interval where the Rayleigh number is between 8 and 65 the convective phenomena are found to be steady and two-dimensional over the length of the cylinder. The flow of the interstitial fluid for this regime of regular two-dimensional convection follows two thermoconvective vortices which are symmetrical about a vertical plane containing the axis of both cylinders. The fluid warms up on contact with the inner cylinder to fall along the outer surface. Heat exchanges are most important on the generatrices $\phi = 0$, $r = r_o$ and $\phi = \pi$ $r = r_i$. The Nusselt number is about 1·5 when $Ra^* = 65$.

(iii) At Rayleigh numbers above 65 a new type of evolution appears: *fluctuating three-dimensional convection*. Perturbations occur in the upper part of the annular layer, and are shown by fluctuations in temperature. The unstable zone is limited by two radial planes, the inclination of which relative to the vertical depends on the Rayleigh number but in no case exceeds the value $\phi = \pm 120°$. The flow remains strictly two-dimensional and steady in the lower part of the cell. A critical Rayleigh number for the transition from *steady two-dimensional convection* to *fluctuating three-dimensional convection* is thus defined. The value chosen is 65 ± 4. It is calculated, on the one hand, by means of thermocouples placed in the field and, on the other, from the diagram of Nu^* *vs.* Ra^* in figure 2: the change in the regime is indeed expressed by a change in the slope due to the increase in heat transfer produced by the instabilities. Figure 3 shows the temperature along the generatrix $\phi = 0$, $r = 1{\cdot}5$ in the middle zone of the model at the Rayleigh number 157 and at the corresponding Nusselt number 2·795. These phenomena are nearly always three-dimensional since the two boundaries represent the temperature of the inner and outer cylinders (T_i and T_o). It will be

noticed that the period P measured on this figure is about 7·5 cm whilst the layer thickness ($\delta = r_o - r_i$) is 4 cm. Hence the ratio $P/2\delta \simeq 0{\cdot}94$. This point will be discussed later together with the study of stability.

The range of investigation extends from 1 to 670 for the Rayleigh number and the experiments were carried out with glass balls 3 and 4 mm in diameter.

The experimental study has not yet enabled us to evaluate exactly the temperature field and the streamlines corresponding to the fluctuating regime since the flow seemed to us to be particularly complex. However, a new convective regime, unexpected in an annular porous layer, could be identified and a critical value of the transition Rayleigh number measured.

4. The perturbation method

An analytical solution of the equations defining the steady two-dimensional regime can give quantitative information about the velocities and the temperature field, as well as the local and total heat transfer. At the same time it makes possible a comparison with the experiment for the steady range at least.

In the system of equations (6) and (7) of § 2, let us take the curl of the two terms of Darcy's equation (7) and introduce the stream function ψ. After some elementary transformations we obtain

$$\nabla^2 T - \mathbf{V}.\nabla T = 0, \tag{8}$$

$$\nabla^2 \psi - Ra^* k = 0, \tag{9}$$

with $$\mathbf{V} = V_r \mathbf{e}_1 + V_\phi \mathbf{e}_2, \quad k = \sin\phi T_{,1} + r^{-1}\cos\phi T_{,2}$$

and $$V_r = r^{-1}\psi_{,2}, \quad V_\phi = -\psi_{,1}$$

(the indices 1 and 2 refer respectively to the vector radius and the normal to it). The boundary conditions may be written as

$$\left.\begin{array}{lllll} \psi = 0 & \text{for} & r = 1, R, & \text{all} & \phi, \\ \psi = 0 & \text{for} & \phi = 0, \pi, & \text{all} & r, \\ T = 1 & \text{for} & r = 1, & \text{all} & \phi, \\ T = 0 & \text{for} & r = R, & \text{all} & \phi, \\ T_{,2} = 0 & \text{for} & \phi = 0, \pi. & & \end{array}\right\} \tag{10}$$

We assume the flow to be symmetrical about the vertical axis and thus consider the range $0 \leqslant \phi \leqslant \pi$. The perturbation method consists of developing T and ψ in power series in the Rayleigh number Ra^*:

$$T = \sum_{m=0}^{\infty} Ra^{*m} T^{(m)}(r, \phi), \tag{11}$$

$$\psi = \sum_{m=1}^{\infty} Ra^{*m} \psi^{(m)}(r, \phi). \tag{12}$$

By introducing the expressions (11) and (12) for T and ψ into the coupled equations (8) and (9) and by identification of the coefficients of each power of Ra^* we obtain

an infinite set of equations which can be solved analytically:

$$\nabla^2 T^{(m)} = \sum_{n=1}^{m} \frac{1}{r} (\psi^{(n)}_{,2} T^{(m-n)}_{,1} - \psi^{(n)}_{,1} T^{(m-n)}_{,2}), \tag{13}$$

$$\nabla^2 \psi^{(m)} = \sin\phi T^{(m-1)}_{,1} + r^{-1} \cos\phi \, T^{(m-1)}_{,2}, \tag{14}$$

with the boundary conditions:

$$\left.\begin{array}{llllllll} T^{(0)} = 1 & \text{for} & r = 1; & \psi^{(m)} = 0 & \text{for} & r = 1, R, & \text{all} & m, \\ T^{(0)} = 0 & \text{for} & r = R; & \psi^{(m)} = 0 & \text{for} & \phi = 0, \pi, & \text{all} & m, \\ T^{(m)} = 0 & \text{for} & r = 1, R, & m \geqslant 1, & & & & \\ T^{(m)}_{,2} = 0 & \text{for} & \phi = 0, \pi, & \text{all} & m. & & & \end{array}\right\} \tag{15}$$

The first equation to be solved is $\nabla^2 T^{(0)} = 0$. The solution satisfying the boundary conditions is

$$T^{(0)} = 1 - C \ln r \quad \text{with} \quad C = (\ln R)^{-1}. \tag{16}$$

Substitution of (16) into (14) with $m = 1$ gives

$$\nabla^2 \psi^{(1)} = -C \sin\phi r^{-1}, \tag{17}$$

the solution of which (found by separation of variables) is

$$\psi^{(1)} = (b_1 r + b_2 r \ln r + b_3 r^{-1}) \sin\phi. \tag{18}$$

The coefficients are determined by means of the boundary conditions (15).

The same process of calculation is continued and gives successively

$$T^{(1)} = (a_1 r \ln^2 r + a_2 r \ln r + a_3 r^{-1} \ln r + a_4 r^{-1} + a_5 r) \cos\phi, \tag{19}$$

$$\psi^{(2)} = (b_4 r^2 \ln^2 r + b_5 r^2 \ln r + b_6 \ln r + b_7 r^2 + b_8 + b_9 r^{-2}) \sin 2\phi, \tag{20}$$

$$\begin{aligned} T^{(2)} = {} & (a_6 r^2 \ln^3 r + a_7 \ln^3 r + a_8 r^2 \ln^2 r + a_9 \ln^2 r + a_{10} r^2 \ln r \\ & + a_{11} \ln r + a_{12} r^{-2} \ln r + a_{13} r^2 + a_{14} + a_{15} r^{-2}) \\ & + (a_{16} r^2 \ln^3 r + a_{17} r^2 \ln^2 r + a_{18} \ln^2 r + a_{19} r^2 \ln r + a_{20} \ln r \\ & + a_{21} r^{-2} \ln r + a_{22} r^2 + a_{23} + a_{24} r^{-2}) \cos 2\phi, \end{aligned} \tag{21}$$

$$\begin{aligned} \psi^{(3)} = {} & (b_{10} r^3 \ln^3 r + b_{11} r \ln^3 r + b_{12} r^3 \ln^2 r + b_{13} r \ln^2 r \\ & + b_{14} r^{-1} \ln^2 r + b_{15} r^3 \ln r + b_{16} r \ln r + b_{17} r^{-1} \ln r \\ & + b_{18} r^3 + b_{19} r + b_{20} r^{-1}) \sin\phi + (b_{21} r^3 \ln^3 r \\ & + b_{22} r^3 \ln^2 r + b_{23} r \ln^2 r + b_{24} r^3 \ln r + b_{25} r \ln r \\ & + b_{26} r^{-1} \ln r + b_{27} r^3 + b_{28} r + b_{29} r^{-1} + b_{30} r^{-3}) \sin 3\phi. \end{aligned} \tag{22}$$

The coefficients a_i and b_i depend only on the ratio of the radii R; the detailed expressions are not given here.

The temperature and stream function at any point may be approximated by the first three terms of the expansions (11) and (12):

$$T = T^{(0)} + Ra^* T^{(1)} + Ra^{*2} T^{(2)}, \tag{23}$$

$$\psi = Ra^* \psi^{(1)} + Ra^{*2} \psi^{(2)} + Ra^{*3} \psi^{(3)}. \tag{24}$$

The perturbation method only holds for sufficiently small values of the Rayleigh number; for the ratio of radii 2, it is shown by experiment that the Rayleigh number must be lower than 75 for coherent results to be obtained.

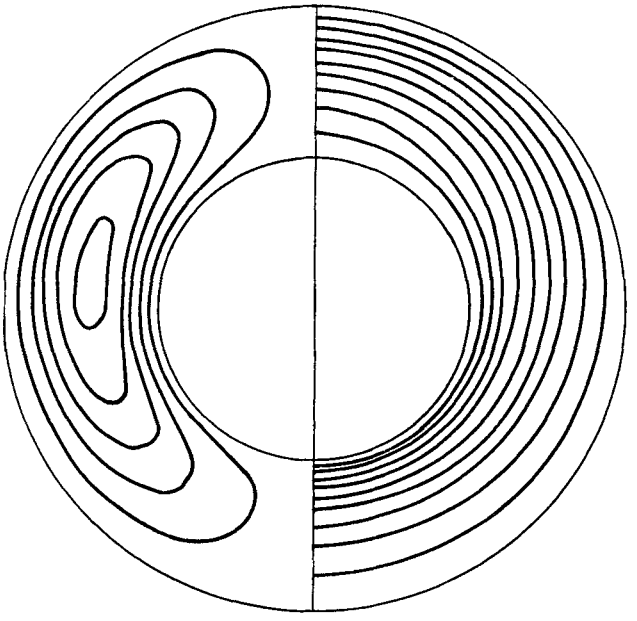

FIGURE 4. Streamlines and temperature field obtained by the perturbation method at $Ra^* = 25$ and $R = 2$.

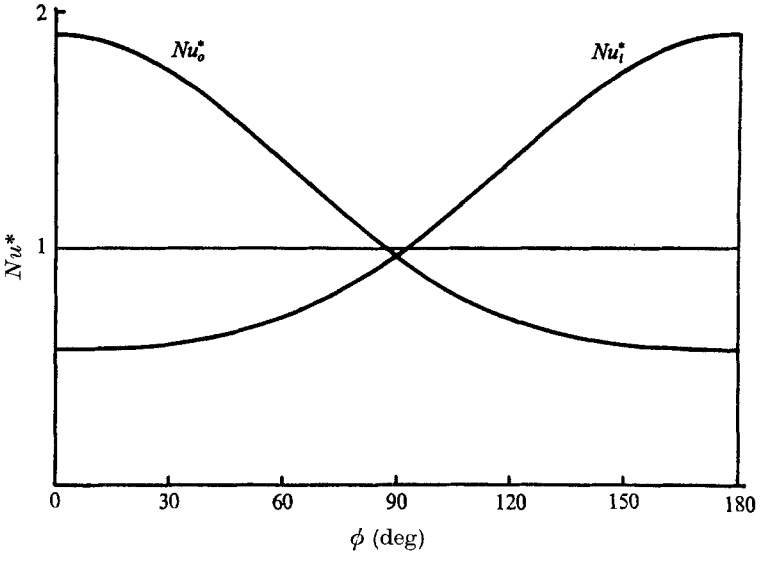

FIGURE 5. Variation of the inside and outside Nusselt numbers Nu_i^* and Nu_o^* with ϕ ($Ra^* = 25$, $R = 2$).

Figure 4 gives an example of the temperature field and streamlines obtained by the perturbation method at the Rayleigh number 25 and at $R = 2$. It is to be noted that at the centre of the vortex, where ψ is a maximum, ψ_c moves towards the upper part of the annular layer ($\phi_c < 90°$).

The local heat transfer at the inner and outer surfaces, as well as the total heat transfer, are given by the following expressions for the Nusselt number:

$$Nu_i^* = -\ln R[rT_{,1}]_{r=1}, \quad Nu_o^* = -\ln R[rT_{,1}]_{r=R}, \tag{25}$$

$$Nu^* = -\frac{\ln R}{\pi}\int_0^\pi [rT_{,1}]_{r=1}d\phi = -\frac{\ln R}{\pi}\int_0^\pi [rT_{,1}]_{r=R}d\phi. \tag{26}$$

Using (23), the total Nusselt number is given by

$$Nu^* = 1 - Ra^{*2}\ln R[a_{10} + a_{11} + a_{12} + 2a_{13} - 2a_{15}]. \tag{27}$$

The local Nusselt numbers are functions of ϕ. The variation in the local Nusselt numbers is shown in figure 5. Heat exchange seems to occur principally in preferential zones.

5. Numerical two-dimensional solution

In order to solve the problem corresponding to the unsteady two-dimensional regime we again consider the system (6) and (7), or equivalently,

$$\partial_t T = \nabla^2 T - \mathbf{V}.\nabla T, \tag{28}$$

$$\nabla^2\psi - Ra^* k = 0. \tag{29}$$

It is of interest that the system contains now only one characteristic number Ra^*. The numerical model consists of this system of equations, suitably discretized, and of a network superimposed on the physical range to be studied. The use of polar co-ordinates transforms the resolution range into a rectangle of width $R-1$ and height 2π. No symmetry about the vertical axis is assumed *a priori*, and the cylindrical annulus is considered as a whole. In this case the boundary conditions may be written as

$$\left.\begin{aligned} &\psi = 0 \quad \text{for} \quad r = 1, R, \quad \text{all} \quad \phi, \\ &T = 1 \quad \text{for} \quad r = 1, \quad \text{all} \quad \phi, \\ &T = 0 \quad \text{for} \quad r = R, \quad \text{all} \quad \phi. \end{aligned}\right\} \tag{30}$$

An initial temperature distribution of the form

$$T_o = 1 - \ln r/\ln R - \alpha \sin(\pi \ln r/\ln R)\cos(s\phi)$$

(α being an amplification coefficient and s a wavenumber) is introduced into the calculation. The number s, in particular, enables us to assign to temperatures asymmetric values with respect to the vertical axis. The stream function is assumed zero initially over the whole range.

The method of alternate directions is used to solve the two coupled equations (28) and (29) on a rectangular network with 49×49 nodes representing the geometrical discretization of the model. A calculation for a given Rayleigh number

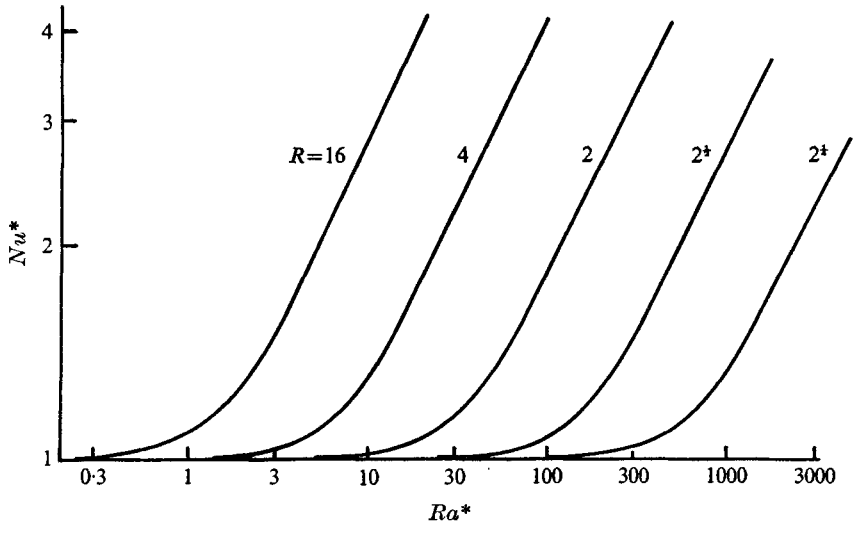

FIGURE 6. Nu^*, Ra^* correlation for five values of the ratio of the radii: $R = 2\frac{1}{4}, 2\frac{1}{2}, 2, 4, 16$.

Ra^* and ratio R is developed as follows. A coherent temperature field is introduced into the calculation. The second term of (29) relative to the stream function is estimated and a convergent iterative process, based on the algorithm of the method of alternate directions, gives the value of the stream function at each node of the network. The velocities are then deduced from the stream function.

The parabolic equation (28) is solved by the same method but the second term in this energy equation includes partial derivatives of the temperature and it is advisable to make iterations within the same time step to determine correctly the temperature field. A cycle corresponding to a new time step is then started. Calculation is continued until the solution is convergent over the whole range. Tests based on the temperature field and at the same time on the global Nusselt number Nu^* then stop the calculation. At every time step the local Nusselt numbers Nu_i^* and Nu_o^*, as well as the total Nusselt number Nu^*, are printed. The time for calculation with the network of 49×49 nodes is 2 s per time step using an IBM 370–168 computer. The number of time steps is of the order of 50. The range of investigation extends from $Ra^* = 0{\cdot}2$ to $Ra^* = 5000$ for five values of the ratio of the radii: $R = 2\frac{1}{4}, 2\frac{1}{2}, 2, 4$ and 16.

The results obtained with a numerical two-dimensional model can be plotted on a graph representing the variation of the Nusselt number Nu^* as a function of the Rayleigh number Ra^* for various values of the ratio R (figure 6). The maximal and minimal numerical values of the local Nusselt numbers calculated at the inner and outer surfaces, together with the maximal stream function, are given in table 1 for various values of Ra^* and R. Whatever the Rayleigh number and the ratio of the radii may be, the solution ultimately exhibits symmetry about the vertical axis, even when the initial conditions are asymmetrical. The unique character of the solution is verified by repeating the same calculation under different initial conditions.

			Nu_i^*		Nu_o^*		
R	Ra^*	Nu^*	min	max	min	max	ψ_{max}
$2^{\frac{1}{4}}$	100	1·0045	0·8708	1·1395	0·8713	1·1435	2·3539
	200	1·0176	0·7532	1·2863	0·7577	1·3005	4·6932
	500	1·1017	0·4758	1·7602	0·4994	1·8351	11·5012
	1000	1·3281	0·2126	2·5518	0·2644	2·8362	21·7615
	2000	1·8193	0·0607	3·8942	0·1028	4·5263	38·4017
	5000	2·9283	0·0062	6·6903	0·0192	8·2966	71·6298
$2^{\frac{1}{2}}$	25	1·0052	0·8616	1·1482	0·8626	1·1568	1·2743
	50	1·0204	0·7349	1·3038	0·7438	1·3326	2·5387
	100	1·0776	0·5215	1·6280	0·5559	1·7354	5·0047
	200	1·2627	0·2464	2·2787	0·3250	2·6829	9·6080
	500	1·9028	0·0410	3·9241	0·0997	5·3525	20·4889
	1000	2·7293	0·0197	5·8701	0·0342	8·2684	32·9472
2	10	1·0172	0·7587	1·2661	0·7651	1·3071	1·1769
	25	1·0993	0·4747	1·6780	0·5267	1·8917	2·8921
	50	1·3278	0·2093	2·3530	0·3031	3·0955	5·4934
	100	1·8286	0·0832	3·5085	0·1340	5·2743	9·7480
	200	2·6256	0·0625	5·2312	0·0545	8·3049	15·8598
	500	4·1983	0·0593	8·7182	0·0243	14·2085	27·0995
4	2	1·0164	0·7874	1·2377	0·7714	1·2937	0·6075
	5	1·0895	0·5558	1·5840	0·5721	1·7780	1·4966
	10	1·3038	0·3257	2·1834	0·3526	2·8852	2·8428
	25	2·0099	0·1930	3·6754	0·1389	6·0025	5·9068
	50	2·9073	0·1785	5·4921	0·0725	9·5514	9·3737
	100	4·1818	0·1802	8·2689	0·0418	14·4234	13·9676
16	0·2	1·0072	0·9048	1·0796	0·8532	1·1658	0·1983
	0·5	1·0266	0·8110	1·2121	0·7622	1·3203	0·4920
	1	1·0927	0·6881	1·4996	0·5911	1·7216	0·9639
	2	1·2965	0·5620	2·0156	0·3842	2·6890	1·7937
	5	1·9528	0·4814	3·5299	0·1801	5·5917	3·5882
	10	2·8138	0·4643	5·6878	0·0992	9·4033	5·5798

TABLE 1. Values of Nu^*, max Nu_i^*, min Nu_i^*, max Nu_o^*, min Nu_o^* and ψ_{max} calculated as a function of Ra^* and R using the numerical two-dimensional model

Two types of evolution are revealed by the numerical analysis and a physical interpretation can be found for each of them. When the Rayleigh number based on the radius of the inside and outside cylinders is less than a certain value (dependent on R), convection is weak. The isotherms for this regime of pseudo-conduction are practically concentric circles. The total Nusselt number is very close to 1.

A second type of evolution, corresponding to the development of convective effects, is to be found as Ra^* increases. In the lower and upper zones of the annular layer the isotherms exhibit deformations which are the greater the more Ra^* is increased. It is also in these regions that the calculated radial velocities are the highest. The curves of Nu^* *vs.* Ra^* in figure 6, plotted in logarithmic co-ordinates, show two zones, characterized by their slopes: the lower part of the curve shows a growing slope, whereas the slope is maximum and constant when the Nusselt

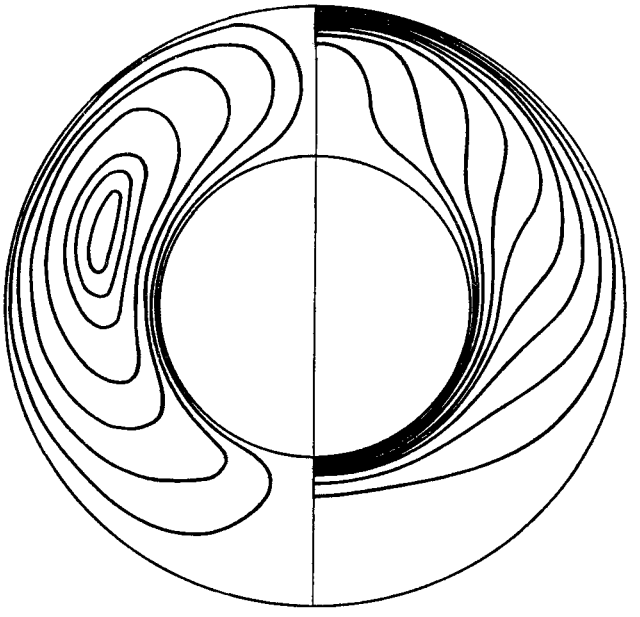

FIGURE 7. Streamlines and temperature field corresponding to $Ra^* = 200$ and $R = 2$.

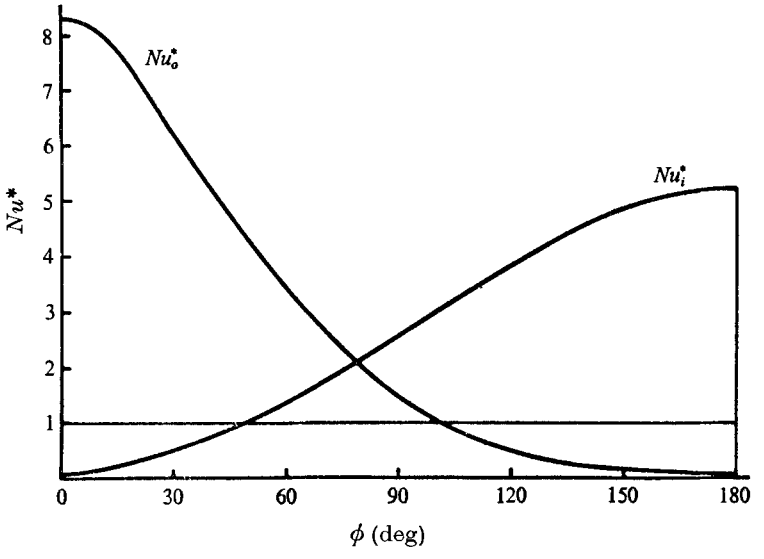

FIGURE 8. Variation of the inside and outside Nusselt numbers Nu_i^* and Nu_o^* with ϕ ($Ra^* = 200$, $R = 2$).

number is above about 1·5. The empirical relation $Nu^* \to A\ Ra^{*0.54}$, where A is a function of R, can describe the evolution in this range. Figure 7 gives an example of the temperature field and streamlines obtained for a Rayleigh number corresponding to this regime of developed regular convection ($Ra^* = 200, R = 2$). The local heat transfer at the inner and outer surfaces, characterized by the two Nusselt numbers Nu_i^* and Nu_o^*, is represented as a function of the angle ϕ for the same Rayleigh number (figure 8). Heat exchanges occur principally in the regions with high temperature gradients, say at $r = 1$, $\phi = 180°$ and at $r = R$, $\phi = 0°$.

The solution of (28) and (29) found using the numerical two-dimensional model is always convergent, whatever the values of Ra^* and R. Expressed in physical terms, this means that natural convection between two cylinders is steady if the porous layer is assumed to be thick. This will be confirmed by the study of stability by Galerkin's technique, to be discussed in § 6.

6. Stability

As the numerical two-dimensional model described in the preceding section does not allow us to reproduce the fluctuating phenomena observed experimentally, a study of stability based on Galerkin's method has been carried out. The results of the numerical model are used to define the initial state on which temperature and velocity perturbations are superposed. This stability study has two aims: first, to determine the critical conditions for the onset of these fluctuating three-dimensional phenomena, and hence a transition critical Rayleigh number Ra_c^* as a function of the ratio of the radii and, second, to get some quantitative information about the influence of the layer length, characterized by the longitudinal aspect ratio $A = L/r_i$, and about the onset of the fluctuations.

Let us again consider the system (1), (4) and (5) in the form

$$\nabla . \mathbf{V} = 0, \tag{31}$$

$$\partial_t T - \nabla^2 T + \mathbf{V} . \nabla T = 0, \tag{32}$$

$$\epsilon^{-1} Pr^{*-1} M^{-1} F \partial_t \mathbf{V} + \nabla p + Ra^* \mathbf{k} T - Ra^* Ga\, \mathbf{k} + \mathbf{V} = 0, \tag{33}$$

with $\mathbf{k} = -\cos\phi\, \mathbf{e}_1 + \sin\phi \mathbf{e}_2$. Consider small perturbations in temperature, velocity, pressure and density:

$$\theta = T - T_0, \quad \mathbf{v} = \mathbf{V} - \mathbf{V}_0, \quad \varpi = p - p_0, \quad -\alpha \Delta T \theta = (\rho - \rho_0)/\rho_1. \tag{34)–(37}$$

The initial two-dimensional state is characterized by the index zero:

$$T_0 = f(r, \phi); \quad \mathbf{V}_0 = h(r, \phi); \quad \mathbf{v} = u\mathbf{e}_1 + v\mathbf{e}_2 + w\mathbf{e}_3. \tag{38}$$

The same simplifying hypotheses as in § 2 are used, in particular the Boussinesq approximation. Let us introduce these perturbations into the system (31)–(33). Then, on taking twice the curl of both terms in (33) and considering

$$Ra^* T_0 \nabla \times \mathbf{k} + \nabla \times \mathbf{v}_0 = 0, \tag{39}$$

we obtain

$$\epsilon^{-1} Pr^{*-1} M^{-1} F \partial_t \nabla^2 \mathbf{v} = Ra^* \mathbf{1} - \nabla^2 \mathbf{v}, \tag{40}$$

where the three components of the vector **l** are given by

$$\left.\begin{aligned} l_1 &= \frac{\cos\phi}{r}\theta_{,1} + \frac{\sin\phi}{r}\theta_{,12} + \frac{\cos\phi}{r^2}\theta_{,22} - \frac{\sin\phi}{r^2}\theta_{,2} + \cos\phi\,\theta_{,33}, \\ l_2 &= -\sin\phi\,\theta_{,11} - \frac{\cos\phi}{r}\theta_{,12} + \frac{\cos\phi}{r^2}\theta_{,2} - \sin\phi\,\theta_{,33}, \\ l_3 &= -\cos\phi\,\theta_{,13} + r^{-1}\sin\phi\,\theta_{,23}. \end{aligned}\right\} \tag{41}$$

Let us multiply the first component of (40) by $\cos\phi$ and the second by $-\sin\phi$ and add:

$$\epsilon^{-1}Pr^{*-1}M^{-1}F\partial_t(\nabla^2 u\cos\phi - \nabla^2 v\sin\phi) = Ra^*\left(\sin^2\phi\,\theta_{,11} + \frac{\cos^2\phi}{r}\theta_{,1} + \frac{\cos^2\phi}{r^2}\theta_{,22} + \theta_{,33}\right) - (\nabla^2 u\cos\phi - \nabla^2 v\sin\phi). \tag{42}$$

If the second-order terms in the energy equation (32) are neglected and we consider

$$\nabla^2 T_0 - \mathbf{V}_0 . \nabla T_0 = 0, \tag{43}$$

equation (32) then becomes

$$\partial_t\theta = \nabla^2\theta - (uT_{0,1} + vr^{-1}T_{0,2}). \tag{44}$$

Equations (42) and (44) form a system whose solution is not *a priori* evident. We make the simplification $\phi = 0$, based on physical considerations. The zone in which perturbations first begin to develop lies, in fact, in the upper part of the annular layer. Further, it is for $\phi = 0$ that the vertical temperature gradients are the greatest. The validity of this hypothesis will be confirmed later.

The system (42)–(44) then reduces to

$$\partial_t\theta = \nabla^2\theta - uT_{0,1}, \tag{45}$$

$$\epsilon^{-1}Pr^{*-1}M^{-1}F\partial_t\nabla^2 u = Ra^*(r^{-1}\theta_{,1} + \theta_{,33}) - \nabla^2 u, \tag{46}$$

with $T_{0,2} = 0$ at $\phi = 0$.

As the porous layer is bounded by two indefinite horizontal and coaxial cylinders, we shall develop the arbitrary perturbation as a function of a one-dimensional periodic wave. The periodic temperature distribution in figure 3 corresponding to a strongly perturbed state supports this hypothesis. Let

$$\theta = \theta(r)\exp(isz), \quad u = u(r)\exp(isz), \tag{47), (48}$$

where $s = m\pi r_i/M$ is the wavenumber and m is the number of cells developed over the length M. θ and u satisfy the boundary conditions $\theta = u = 0$ for $r = 1$ and $r = R$. The equations then become

$$\partial_t\theta = (D^2 + r^{-1}D - s^2)\theta - T_{0,1}\,u, \tag{49}$$

$$\epsilon^{-1}Pr^{*-1}M^{-1}F\partial_t(D^2 + r^{-1}D - s^2)u = Ra^*(r^{-1}D - s^2)\theta - (D^2 + r^{-1}D - s^2)u, \tag{50}$$

with $D = d/dr$ and the dimensionless numbers defined above.

The Galerkin method (Kantorovich & Krylov 1958; Finlayson 1972) applied here to solve this system consists of representing the perturbations θ and u by a

set of linearly independent functions satisfying the boundary conditions in the form

$$\theta = \sum_{i=1}^{N} a_i(t)\Theta_i(r), \quad u = \sum_{i=1}^{N} b_i(t)U_i(r). \tag{51), (52}$$

Let us introduce these expressions for θ and u into the system (49) and (50), multiply the two equations by Θ_j and U_j, respectively, and integrate over the layer thickness. We then have

$$A_{ij}\,da_i/dt = B_{ij}a_i + C_{ij}b_i, \tag{53}$$

$$D_{ij}\,db_i/dt = Ra^* E_{ij}a_i + F_{ij}b_i, \tag{54}$$

where A_{ij}, B_{ij}, D_{ij}, E_{ij} and F_{ij} are constants and C_{ij} is a term which depends on the initial temperature distribution in the layer. In the present case, $T_0(r, \phi)$ is defined by the numerical two-dimensional model developed in § 5. Standard manipulations give, for example,

$$B_{ij} = -\int_1^R \left(DU_i\,DU_j - \frac{1}{r}DU_i U_j + s^2 U_i U_j\right) dr\ldots,$$

$$C_{ij} = -\int_1^R U_i \Theta_j T_{0,1}\,dr.$$

The differential system of $2N$ equations with constant coefficients can be reduced to the form

$$d\mathbf{C}/dt = \mathbf{A}^{-1}\mathbf{B}\mathbf{C} = \mathbf{L}\mathbf{C}, \tag{55}$$

where **A**, **B** and **L** are square matrices and **C** the column matrix of the coefficients. The solution of the differential system (55) may be written as

$$C_j = c_j \exp(\lambda_j t) \quad (j = 1, 2, \ldots, 2N). \tag{56}$$

The necessary and sufficient condition for the system to be asymptotically stable is that the eigenvalues of the matrix **L** have a real negative part (the imaginary part being null at the marginal state; Glansdorff & Prigogine 1971). The characteristic equation takes the form (with **I** the identity matrix)

$$\det(\mathbf{L} - \lambda\mathbf{I}) = 0. \tag{57}$$

The limiting state between stable two-dimensional and unstable three-dimensional states may be defined by the Routh–Hurwitz criterion, which for dissipative systems such as the one studied here amounts to cancelling the determinant of the matrix **B** (Finlayson 1972) contained in (55):

$$\begin{vmatrix} B_{ij} & C_{ij} \\ Ra^* E_{ij} & F_{ij} \end{vmatrix} = 0. \tag{58}$$

It is to be noticed that in our case the search for the marginal state and, in particular, the determination of the stability criterion are carried out from an initial state in which the convective phenomena are already highly developed. To use the method described above it is necessary to know the temperature field. We could obtain it by direct measurements on an experimental outfit, but in our

	$N = 1$		$N = 2$		$N = 3$	
R	$\mathscr{R}a_c^*$	α_c	$\mathscr{R}a_c^*$	α_c	$\mathscr{R}a_c^*$	α_c
$2^{\frac{1}{4}}$	40·698	3·1713	40·202	3·1633	40·202	3·1637
$2^{\frac{1}{2}}$	43·145	3·1985	42·789	3·1840	42·789	3·1844
2	65·943	3·3079	67·057	3·3122	66·962	3·3122
4	216·92	3·7573	227·52	3·8550	228·47	3·8310

TABLE 2. Critical transition Rayleigh number $\mathscr{R}a_c^*$ and critical wavenumber α_c calculated for $R = 2^{\frac{1}{4}}, 2^{\frac{1}{2}}, 2, 4$ and with the approximations $N = 1, 2, 3$

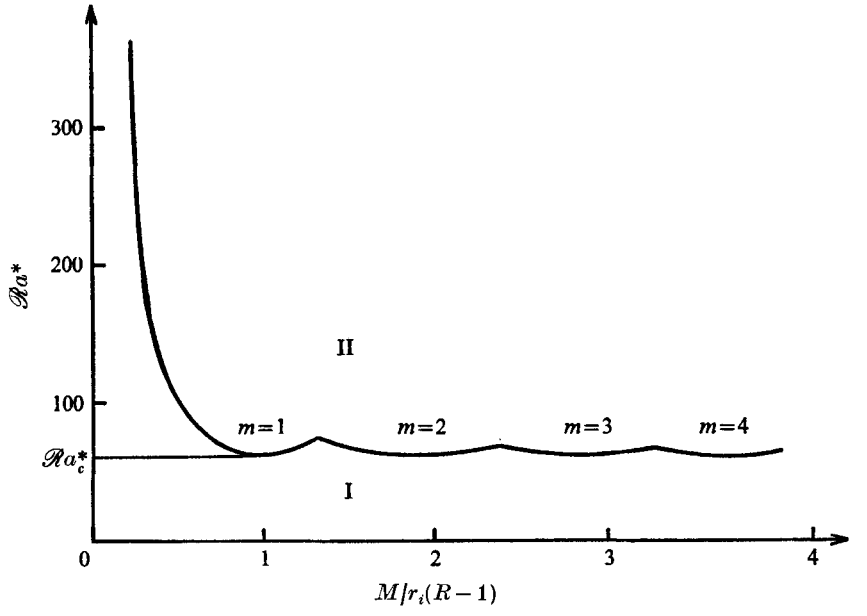

FIGURE 9. The Rayleigh number $\mathscr{R}a^*$ as a function of the length M for $R = 2$.

case the temperature distribution T_0 is calculated using the numerical two-dimensional model.

We shall now describe the way in which the critical Rayleigh number Ra_c^* for the onset of fluctuating three-dimensional phenomena has been calculated.

A numerical calculation is performed with a Rayleigh number chosen arbitrarily and the value of R at which the critical conditions are sought. The temperature distribution obtained after convergence of the calculation is inserted into the differential system (53) and (54). The different integrals A_{ij}, B_{ij}, C_{ij}, D_{ij}, E_{ij} and F_{ij} are calculated numerically and the minimum critical Rayleigh number Ra_c^* is determined as a function of the wavenumber s. The value of the critical wavenumber corresponding to a minimal Ra_c^* is thus found. A numerical calculation is started with this new value of Ra_c^* and so on, until the process becomes convergent. The critical conditions defined are characterized by the value of the minimal critical Rayleigh number Ra_c^* and by the wavenumber

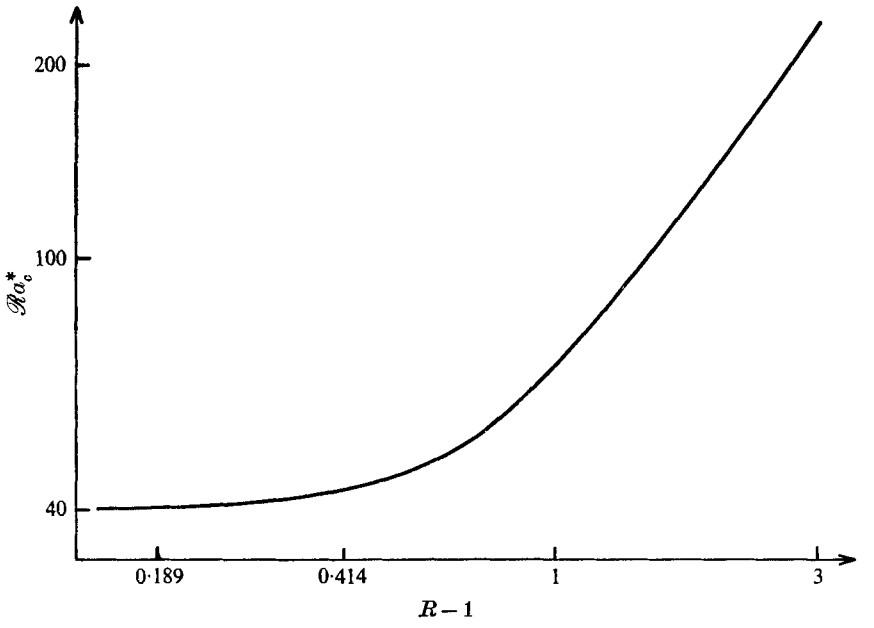

FIGURE 10. The critical transition Rayleigh number $\mathscr{R}a_c^*$ as a function of $R-1$.

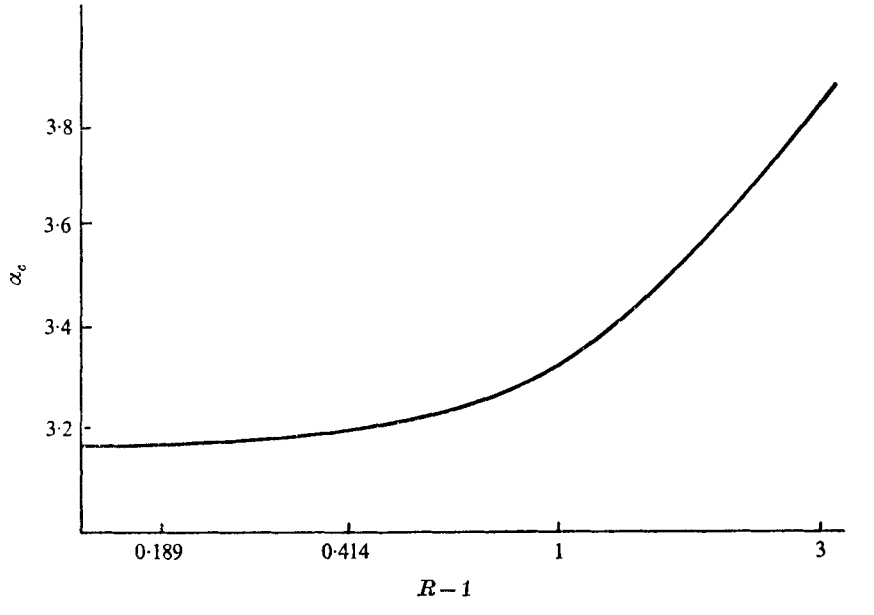

FIGURE 11. The wavenumber α_c as a function of $R-1$.

corresponding to $s_c = m\pi r_i/M$. The values of the critical Rayleigh numbers $\mathscr{R}a_c^* = Ra_c^*(R-1)$ and the wavenumbers $\alpha_c = s_c(R-1)$ based on the thickness $r_o - r_i$ of the layer are reported in table 2 for four values of the ratio of the radii R and a set of trial functions satisfying the boundary conditions:

$$\Theta_i = U_i = [(\ln R - \ln r)\ln r]^i.$$

Figure 9 illustrates the variation of the Rayleigh number $\mathscr{R}a^*$ as a function of $M/r_i(R-1)$ at $R = 2$ for a number of cells chosen such that $\mathscr{R}a^*$ is a minimum. Range I corresponds to a steady two-dimensional regime, range II to the fluctuating three-dimensional regime. If the length of the annular layer M ($\alpha = m\pi(r_0 - r_i)/M$) is taken equal to zero, which corresponds to the numerical two-dimensional model, the transition critical Rayleigh number is then infinite.

The variation of $\mathscr{R}a_c^*$ and α_c as functions of $R-1$ are shown in figures 10 and 11. When the ratio R tends to 1 the curve $\mathscr{R}a_c^*(R)$ tends to the limit corresponding to the onset of natural convection in a horizontal porous layer, i.e. to $4\pi^2$. The wavenumber tends to π.

The critical Rayleigh number $\mathscr{R}a_c^*$ and the wavenumber α_c given in table 2 are found to increase for larger values of R. The value obtained at $R = 2$ may be compared with the critical Rayleigh number and the critical wavenumber found experimentally: $\mathscr{R}a_c^* = 65 \pm 4$ and $\alpha_c = 3{\cdot}27$.

7. Numerical three-dimensional solution

From the results of the stability study we are led to construct a numerical three-dimensional model in order to approach the fluctuating phenomena.

We again consider the system (6) and (7), in rectangular co-ordinates. The energy equation becomes

$$\partial_t T = \nabla^2 T - \mathbf{V}.\nabla T. \tag{59}$$

Taking the curl of the two terms in (7) makes the pressure term disappear.

As the medium is supposed to be incompressible ($\nabla.\mathbf{V} = 0$) the field is solenoidal and thus we can set $\mathbf{V} = \nabla \times \boldsymbol{\psi}$, where $\boldsymbol{\psi}$ is a vector potential which can always be assumed to be solenoidal also ($\nabla.\boldsymbol{\psi} = 0$) (Hirasaki & Hellums 1968; Holst & Aziz 1971). Thus

$$\nabla^2\boldsymbol{\psi} = \mathbf{k} = Ra^*(T_{,2}\,\mathbf{e}_1 - T_{,1}\,\mathbf{e}_2). \tag{60}$$

With the assumption $\psi_1 = 0$ at $r = 1$ and $r = R$ and with $\nabla.\boldsymbol{\psi} = 0$, the boundary conditions are

$$\left.\begin{aligned} &\psi_{1,1} = 0, \quad \psi_2 = \psi_3 = 0 \quad \text{for} \quad x = 0, A, \quad \text{all} \quad r, \\ &\psi_1 = 0, \quad \psi_{2,n} + \psi_2 = 0, \quad \psi_{3,n} + \psi_3 = 0 \quad \text{for} \quad r = 1, R, \quad \text{all} \quad x, \end{aligned}\right\} \tag{61}$$

where $A = L/r_i$ is the longitudinal aspect ratio of the cell and $\psi_{i,n}$ the derivative normal to the surface of the component ψ_i.

The choice of rectangular co-ordinates proceeds from the method of finite elements used here. This method offers, among other things, flexibility as to choice of geometrical model: the modification relative to a shift in configuration amounts to giving the new co-ordinates of the network nodes and, eventually, new boundary conditions.

So we try to solve the system consisting of one equation of parabolic type (59) and three Poisson equations (60). In fact, with the boundary conditions stated, the solution of the third equation $\nabla^2\psi_3 = k_3 = 0$ is identically zero.

From a physical viewpoint the finite-element method consists of dividing the range of investigation V into geometrically simple subdomains V_E. These elements are then juxtaposed to give the total domain and the approximate solution (Wilson & Nickell 1966).

In order to get a strict mathematical formulation of the finite-element method, several approaches are possible; one of them is approximation by minimization of the functional corresponding to the problem, but this method is not available for the situation where the functional does not exist or has not been found, or cannot be minimized (Finlayson & Scriven 1967). For our study we have chosen the direct process of Galerkin (Finlayson 1972; Zienkiewicz 1971).

Let us consider the equations governing the variation of the function u in the volume V and its evolution in time:

$$A(u) = 0 \quad \text{in } V \quad (t > 0), \tag{62}$$

with the boundary conditions and initial conditions

$$\left.\begin{aligned} C(u) &= 0 \quad \text{on} \quad S \quad (t > 0),\\ D(u) &= 0 \quad \text{in} \quad V \quad (t \leqslant 0), \end{aligned}\right\} \tag{63}$$

A, C and D being operators.

A solution of (62) is given as a trial function satisfying the boundary conditions

$$u_n = N\{u\}, \tag{64}$$

where N is a shape function representative of interpolation and depending on space and time co-ordinates, and $\{u\}$ is a set of n parameters. The trial function (64) is introduced in (62) and the weighted residuals become

$$\int_V W_k R\, dV = 0 \quad (k = 0, 1, 2, \ldots, n), \tag{65}$$

where the residual $R = A(u_n)$ must be zero when the trial function is the exact solution of the problem governed by $A(u)$; W_k is the weight function.

In the Galerkin process, the weight function is the shape function N which defines the approximation

$$\int_V N_i\, A(N\{u\})\, dV = 0. \tag{66}$$

If the operator corresponds to the energy equation, then

$$\nabla . (\mathbf{k}\nabla u) + Q = \partial_t u. \tag{67}$$

If k_1, k_2 and k_3 are the non-vanishing components of thermal-conductivity tensor $\mathbf{k}$, which is supposed diagonal and independent of temperature, the integral (66) applied to the volume V becomes

$$\int_V N_i\{-[(k_1 u_{,1})_{,1} + (k_2 u_{,2})_{,2} + (k_3 u_{,3})_{,3}] - Q + \partial_t u\}\, dV = 0 \tag{68}$$

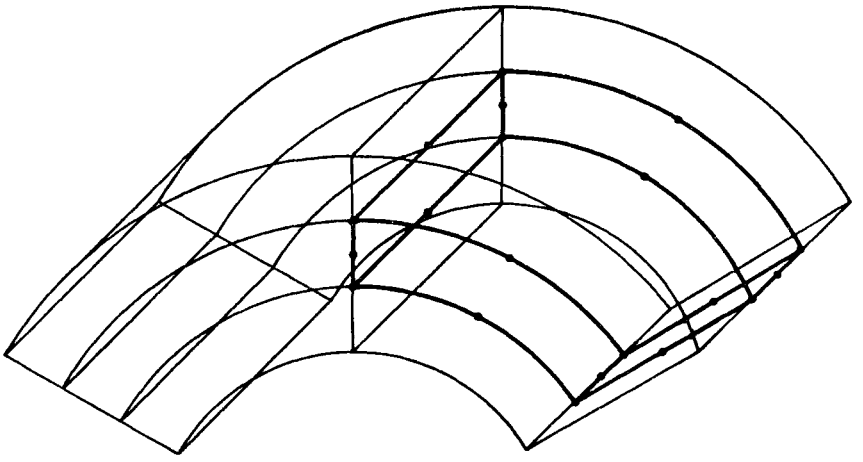

FIGURE 12. Details of three-dimensional network.

when the boundary conditions $C(u)$ on S are of Dirichlet type. For a linear interpolation of the function u in time over the range $[t_0, t_1] = \Delta t$, the function u_n is written as

$$u_n = [N_0, N_1] \begin{bmatrix} \{u\}_0 \\ \{u\}_1 \end{bmatrix} \quad \text{with} \quad N_0 = (\Delta t - t)/\Delta t, \quad N_1 = t/\Delta t; \tag{69}$$

$\{u\}_0$ and $\{u\}_1$ are the column matrices of nodal values at t_0 and t_1, $\{u\}_0$ being known at the instant t_0.

The u derivative is

$$\partial_t u = [\partial_t N_0, \partial_t N_1] \begin{bmatrix} \{u\}_0 \\ \{u\}_1 \end{bmatrix} = 1/\Delta t[-1, 1] \begin{bmatrix} \{u\}_0 \\ \{u\}_1 \end{bmatrix}. \tag{70}$$

Let us substitute expressions (69) and (70) for u and $\partial_t u$ in (68) and integrate from 0 to $\Delta t (t_0 = 0)$; finally we obtain a linear system in matrix form:

$$\mathbf{G}\{u\}_1 = \mathbf{S}, \tag{71}$$

with $$\mathbf{G} = \tfrac{2}{3}\mathbf{H} + (\Delta t)^{-1}\mathbf{C}, \quad \mathbf{S} = \mathbf{P} - (\tfrac{1}{3}H - (\Delta t)^{-1}\mathbf{C})\{u\}_0,$$

where $$H_{ij} = \int_V (k_1 N_{i,1} N_{j,1} + k_2 N_{i,2} N_{j,2} + k_3 N_{i,3} N_{j,3})\, dV,$$

$$C_{ij} = \int_V N_i N_j dV, \quad P_i = \int_V Q N_i dV.$$

These integrals are evaluated numerically when the elementary domains are curved.

The linear system (71) is then solved using an iterative or direct method, depending on the type of element considered. The numerical model consists of several parts, allowing successively the network to be generated, the elementary matrices to be calculated and assembled, and the system to be solved by the Cholevsky method by bands.

The physical range is represented by an assembly of curved isoparametric

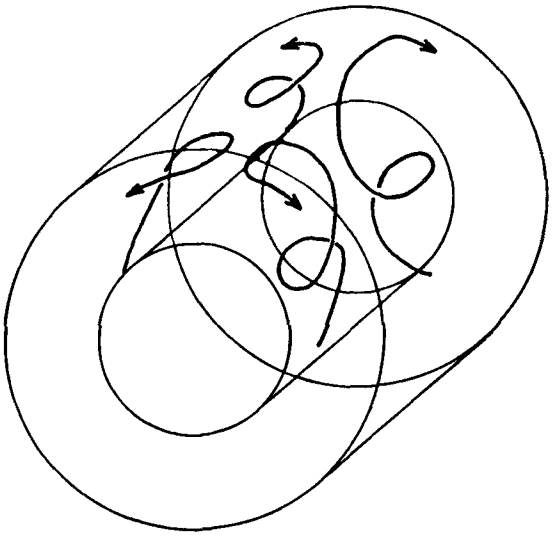

FIGURE 13. Streamlines corresponding to the fluctuating three-dimensional regime.

elements with 20 nodes. This network is made up of 54 elements and 336 nodes. Figure 12 shows the element arrangement in the annular layer.

In view of the problem considered (transitory three-dimensional) the computer program is too long. Therefore calculations for only three Rayleigh numbers (50, 100 and 200) have been carried out for the ratio of the radii 2.

An initial temperature distribution is inserted into the calculation, i.e.

$$T_o = 1 - \ln r/\ln R + \alpha_1 \sin(\pi \ln r/\ln R)\sin(s_1 \tilde{\phi}),$$

with $\tilde{\phi} = \phi + \alpha_2 \pi \cos(s_2 \pi z)$, where α_1 and α_2 are amplification coefficients and s_1 and s_2 wavenumbers characteristic of the initial perturbation.

Two different types of evolution are obtained, depending on the value of the Rayleigh number. At the Rayleigh number 50 the initial three-dimensional perturbation is found to disappear gradually during evolution to give place to strictly two-dimensional temperature and velocity fields. Further, the calculation is found to converge to a stable solution corresponding to that of the two-dimensional model. In particular, the Nusselt numbers are equal to within the errors of calculation. At the Rayleigh numbers 100 and 200 the evolution is different: the initial perturbation grows in the course of time and the three-dimensional effects are more pronounced. The flow remains two-dimensional on the lower part of the curve, whereas it displays spiral deformations on the upper part. Some streamlines are shown in figure 13. Convergence to a stable solution could not be obtained in the intervals of time considered.

It was not possible to proceed to a more accurate control of the value of the critical Rayleigh number dividing the two convective regimes because of the long calculation which would have been necessary to eliminate the influence of the arbitrary initial conditions. In spite of the small number of calculations performed, this numerical study allowed us to find the two thermoconvective

regimes, the steady two-dimensional one and the fluctuating three-dimensional one, observed in experiments and expected theoretically from the study of stability.

8. Physical interpretation

The study of stability enables us to get a better understanding of the reason why the two-dimensional theory only mentions steady convective phenomena, contrary to what is observed with a horizontal layer: with $N = 1$, for example, condition (58) becomes

$$BF - Ra^* CE = 0; \quad \text{hence} \quad Ra^* = \frac{BF}{CE} = \frac{(I_1 - I_2 + s^2 I_3)^2}{(I_2 - s^2 I_3) I_4},$$

where I_1, I_2, I_3 and I_4 are integrals with definite values and $s = m\pi r_i/M$, with $m \neq 0$ ($m = 0$ corresponds to the two-dimensional regime). The number M, which represents the length of the annular layer, is zero in our case. As the Rayleigh number is proportional to s^2 when s increases to infinity the unstable regime can never be obtained, as can be seen also in figure 9.

Let us now try to analyse from a physical point of view the mechanisms generating the secondary three-dimensional effects. Owing to the existence of a gradient between the two cylinders, more or less important motions are produced in the fluid depending on the value of this gradient and on the other experimental parameters. By contrast, in a horizontal porous layer convective phenomena are found to occur only from a marginal state resulting from a competition between the stabilizing dissipative effects and, on the other hand, the destabilizing convective effects. However, both configurations are not so different far from equilibrium, as the Rayleigh number increases: the horizontal porous layer is then the seat of important convective phenomena which develop in the form of organized cells and at certain points high gradients are found to appear which are sufficient for the critical conditions for the onset of convection to be reached locally (Caltagirone 1975*b*). Whenever the critical conditions are exceeded at any point the perturbation develops in the form of micro-vortices. The fluctuating regime then results from the interaction of these micro-vortices with the main stream representing a thermoconvective cell.

The same holds for the annular cylindrical layer. The critical conditions for the occurrence of local perturbations in a medium where convective phenomena are already highly developed are met when the energy released by the forces due to the adverse thermal gradient compensates the energy dissipated by conduction and convection. The instability thus appears as a competition between the two mechanisms.

The Nu^*, Ra^* diagram in figure 14 reproduces the results obtained successively from the experimental study, with the perturbation method and with the numerical model for $R = 2$. As long as the convection regime is steady the experimental points more or less accurately lie on the theoretical curve relative to the two-dimensional model. When the Rayleigh number is above 65, practically all the experimental points are above this theoretical curve, showing the increase

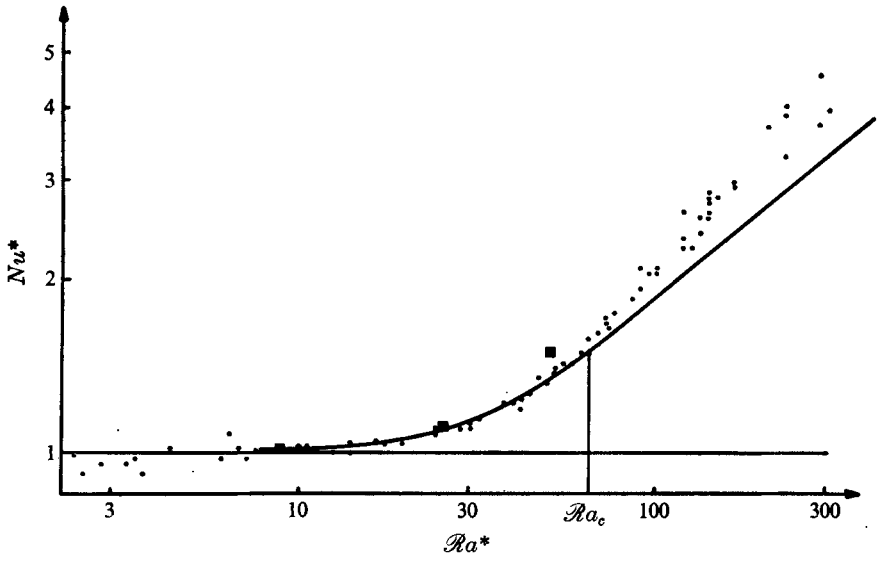

FIGURE 14. Comparison of the results obtained from experiments (asterisks), from the perturbation method (squares) and from the numerical model (curves) on the Nu^*, Ra^* diagram for $R = 2$.

in heat transfer due to the instabilities. The Nu^*, Ra^* curve obtained by the perturbation method coincides with that obtained with the numerical model at low Rayleigh number and deviates from it as this number increases.

9. Conclusions

The results for natural convection in a porous layer bounded by two horizontal concentric cylinders which are reported in this paper have been obtained by a physical and mathematical approach to the problem.

The experimental study has pointed out the complexity of the phenomena owing to the existence of different thermoconvective regimes according to the values of the experimental parameters. The critical Rayleigh number separating the regime of regular two-dimensional convection from that of fluctuating three-dimensional convection has thus been defined: at $R = 2$, $\mathscr{R}a_c^* = 65$. In order to approach the physical reality a mathematical formulation of the physical system has been given and the equations obtained have been solved by different methods.

The study of stability in an annular layer shows the importance of the third dimension for the occurrence of these perturbations and gives, furthermore, the value of the critical transition Rayleigh number as a function of the ratio of the radii: at $R = 2$, $\mathscr{R}a_c^* = 66{\cdot}96$.

The good agreement between experimental and theoretical Rayleigh numbers results from several causes: the equations used are very representative as in many other problems and, on the other hand, Galerkin's method is very general and very efficient in the search for criteria for hydrodynamic stability.

However, an experimental description of the phenomenon is not sufficient. Only an exhaustive study will enable us to classify the different convective regimes and to verify the theory. In the same way, a more complete exploitation of the three-dimensional model can contribute to defining the temperature field and the streamlines for each thermoconvective regime.

I should like to thank here the Department of Rocks Mechanics of the Laboratoire Central des Ponts et Chaussées for kindly providing the finite-element computer program used here after modification for the treatment of coupled transitory problems. I am very grateful to Professor J. J. Bernard, Director of the Laboratoire d'Aérothermique du C.N.R.S., for encouragement and helpful assistance.

REFERENCES

ABBOTT, M. R. 1964 *Quart. J. Mech. Appl. Math.* **17**, 471.

BISHOP, E. H. & CARLEY, C. T. 1966 *Proc. Heat Transfer Fluid Mech. Inst.*, p. 63. Stanford University Press.

BISHOP, E. H., CARLEY, C. T. & POWE, R. E. 1968 *Int. J. Heat Mass Transfer*, **11**, 1741.

BORIES, S. A. & COMBARNOUS, M. A. 1973 *J. Fluid Mech.* **57**, 63.

CALTAGIRONE, J. P. 1971 *Mém. CNAM, Paris.*

CALTAGIRONE, J. P. 1972 *C.R. Acad. Sci. Paris*, **275**, 307.

CALTAGIRONE, J. P. 1975*a* 6 *ème Cong. Int. Fondation Française d'Etudes Nordiques, Le Havre* (to be published).

CALTAGIRONE, J. P. 1975*b* *J. Fluid Mech.* **72**, 269.

CHANDRASEKHAR, S. 1961 *Hydrodynamic and Hydromagnetic Stability.* Oxford: Clarendon Press.

CLOUPEAU, M. & KLARSFELD, S. 1973 *Appl. Optics*, **12**, 198.

COMBARNOUS, M. A. & BORIES, S. A. 1975 *Adv. in Hydrosci.* **10**, 231–307.

CRAWFORD, L. & LEMLICH, R. 1962 *Indust. Engng Chem. Fund.* **1**, 260.

FINLAYSON, B. A. 1968 *J. Fluid Mech.* **33**, 201.

FINLAYSON, B. A. 1972 *The Method of Weighted Residuals and Variational Principles.* Academic.

FINLAYSON, B. A. & SCRIVEN, L. E. 1967 *Int. J. Heat Mass Transfer*, **10**, 799.

GLANSDORFF, P. & PRIGOGINE, I. 1971 *Structure, Stabilité et Fluctuations.* Masson.

GRIGULL, U. & HAUF, W. 1966 *Proc. 3rd Int. Heat Transfer Conf.*, paper 60, vol. 2, p. 182.

HIRASAKI, G. J. & HELLUMS, J. D. 1968 *Quart. Appl. Math.* **16**, 331.

HOLST, P. H. & AZIZ, K. 1971 *Int. J. Heat Mass Transfer*, **15**, 73.

KANTOROVICH, L. V. & KRYLOV, V. I. 1958 *Approximate Methods in Higher Analysis.* Noordhoff.

LIS, J. 1966 *Proc. 3rd Int. Heat Transfer Conf.*, paper 61, vol. 2, p. 196.

LIU, C. Y., MUELLER, W. K. & LANDIS, F. 1961 *Int. Dev. Heat Transfer*, paper 117, pt 5, p. 976. A.S.M.E.

MACK, L. R. & BISHOP, E. H. 1968 *Quart. J. Mech. Appl. Math.* **21**, 223.

POWE, R. E., CARLEY, C. T. & CARRUTH, S. L. 1971 *J. Heat Transfer, Trans. A.S.M.E.* **93**, 210.

ROTEM, Z. 1971 *Int. J. Heat Mass Transfer*, **15**, 1679.

WILSON, E. L. & NICKELL, R. E. 1966 *Nucl. Engng Design*, **4**, 276.

ZIENKIEWICZ, O. C. 1971 *The Finite Element Method in Engineering Science.* McGraw-Hill.